Korean J. Chem. Eng., **29**(1), 25-35 (2012)
DOI: 10.1007/s11814-011-0130-5

Application of simulated annealing (SA) to the synthesis of heterogeneous catalytic reactor

Sungwon Hwang*,† and Robin Smith**

*Process, Technology and Engineering, UOP Ltd., Liongate, Ladymead, Guildford, Surrey, GU1 1AT, UK
**Centre for Process Integration, School of Chemical Engineering and Analytical Science,
The University of Manchester, P. O. Box 88, Manchester, M60 1QD, UK
(*Received 3 April 2011 • accepted 11 May 2011*)

Abstract−This paper reviews a practical application of the optimization algorithm to conceptual design of a heterogeneous catalytic reactor and catalyst and its synthesis. In particular, a simulated annealing (SA) algorithm is mainly used since it provides a reliable optimization solution without being trapped at local optimum points, which arise from non-convexities and multiplicities in a complex reaction system. Furthermore, it allows a design engineer to evaluate multiple design options of reactor and catalyst systems which satisfy both user-specified objective functions and constraints. In the final stage of optimization, these generated solutions are fine-tuned by using deterministic optimization. To enhance the efficiency of optimization further, a profile-based synthesis is adopted for the optimization algorithm. Lastly, this research takes into account a number of factors for the synthesis of heterogeneous catalytic reactors such as reactor configuration, uniform and non-uniform catalyst type, and fundamental catalyst design parameters including shape and its definite dimensions.

Key words: Catalyst, Reactor, Optimization, Simulated Annealing, Modelling

INTRODUCTION

Many different types of optimization algorithms have been developed and applied to systematic process design in chemical engineering. Each optimization algorithm has its own advantages and disadvantages, and it is essential to understand the nature of each algorithm and to ensure if an appropriate tool is employed for the system design. In broad terms, optimization can be divided into two different categories: deterministic and stochastic optimization. The most well-known algorithm of deterministic optimization is successive quadratic programming (SQP) for non-linear problems, whilet various stochastic optimizations have been developed such as simulated annealing, genetic algorithms, neural networks, tabu search, and target analysis.

Deterministic algorithms such as successive quadratic programming (SQP) can in principle find a global optimization solution very fast for a continuous and non-linear problem. However, limitations arise when the problem belongs to MINLP (mixed integer non-linear programming) models. Furthermore, these conventional deterministic optimization methods show frequent traps to local optimal points in a highly non-linear problem of reactor synthesis.

In the present study, simulated annealing (SA), which utilizes stochastic optimization, is used for the synthesis of reactor and heterogeneous catalyst. The main advantage of using this stochastic algorithm is that the global optimization point can be reached regardless of the initial starting point, since the algorithm incorporates probabilistic elements both in the problem and algorithm itself in contrast to deterministic optimization. Furthermore, the algorithm provides various design solutions that satisfy the objective function and constraints. Therefore, various types of novel reactor and catalyst designs can be developed from the optimization results. However, this method suffers from a relatively large computation time for the optimization compared with deterministic algorithms. For this reason, an innovative approach is used in this work to maximize the use of powerful functions of these two individual algorithms. For example, a simulated annealing (SA) method is mainly used at initial stage of optimization to find a set of feasible optimum solutions, while the obtained premature solutions are fine-tuned by using a SQP (successive quadratic programming) algorithm at final stage. Furthermore, a profile-based synthesis approach is adopted in order to increase the efficiency of the optimization algorithm further.

For illustration, the modelling of a non-uniform catalyst and its synthesis with a heterogeneous catalyst reactor in ethylene oxidation process is represented.

†To whom correspondence should be addressed.
E-mail: Sungwon.hwang@uop.com

BACKGROUNDS

1. Simulated Annealing (SA)

As defined in its name, simulated annealing exploits the basic concept from the process of metal annealing. Physical metal annealing is a process of transforming from high energy in liquid to low energy status in a solid by initially melting the substance and decreasing temperature slowly, spending long time near the freezing point. In the liquid state, particles are distributed randomly. However, a stable crystalline state is formed with a minimum energy configuration corresponding to the one of the solid. In the process of annealing, the solid cannot reach the minimum energy status if the cooling is not done slowly enough, and it becomes unstable like a glass or a crystal with several defects in the structure. Furthermore, the resulting solids at different energy conditions of the simulated annealing method refer to different feasible solutions in the

combinatorial optimization problem, and the energy of the solid corresponds to the objective function, which is to be minimized.

The approach of simulated annealing is based on simple algorithm of Metropolis et al., which originally introduced the methods to find the equilibrium configuration of a collection of atoms at a given temperature [1]. The connection between this algorithm and mathematical minimization was first noted by Pincus and Kirkpatrick et al. who proposed the optimization technique for combinatorial problems [2,3]. Since then, simulated annealing has been applied to various optimization problems in areas such as computer design, image screening, molecular physics, chemistry, process design, and so on [4]. Apart from simulated annealing, other heuristic search methods have also been developed, such as genetic algorithms, neural networks, tabu search and target analysis. These heuristic search methods are summarized by Glover and Greenberg [5]. These optimization methods produce good solutions but not necessarily a global optimum solution, within a reasonable computing time. Simulated annealing has also been extended to optimization problems with continuous variables, and the summary of these approaches can be found in the work of Van Laarhoven and Aarts [6].

The major advantage of simulated annealing is an ability to avoid being trapped at a local optimum point during optimization. The algorithm employs a random search accepting not only the change that improves the objective function but also the changes that deteriorate it.

2. Logical Theory of Simulated Annealing (SA)

Simulated annealing is a modification of a local search algorithm. A brief procedure of local search algorithm follows.

1. Select an initial state at i and calculate f(i).
2. Generate neighbor, j, in a random manner and calculate f(j).
3. Calculate δ (=f(j)− f(i)), comparing current result with previous result.
4. Replace the result if the current result is better than previous result.
5. Repeat steps 2 to 4.
6. Stop.

Even though this local search algorithm is simple and quick to execute, the main disadvantage of this method is that the solution might be far from any global optimum point. A possible solution to this problem is to exploit multiple starting points to produce different optimum results, and the best optimum solution among the resulting products can be regarded as a global optimum point. In a similar approach, the simulated annealing avoids being trapped in a local optimum point by sometimes accepting the neighbors, producing results which go in the opposite direction of the optimum point. The acceptance or rejection of these opposite moves is determined by a sequence of random numbers but with a controlled probability. The probability of acceptance for the move, which goes away from the optimum point, is called the acceptance function. It is generally set to exp(−δ/T), where T is a cooling temperature. In principle, a small increase of the objective function of f is more likely to be accepted than a large increase, for example, in the case of minimization of f. Also, most moves are accepted at a high temperature, while most increase moves are rejected as temperature approaches to freezing point. For this reason, the algorithm starts with high initial temperature in order to avoid a premature trap in a local optimum point during optimization. A certain number of neighborhood moves are applied at each temperature, while the temperature parameter is gradually decreased. This modified algorithm of local search is as follows.

Step 1. Select an initial state at i and calculate f(i).

Step 2. Select an initial temperature, T^o.

Step 3. Set repetition counter (Markov chain length).

Step 4. Generate neighbor, j, in a random manner and calculate f(j).

Step 5. Calculate δ (=f(j)− f(i)), comparing current result with the previous result.

Step 6. Replace the result if the current result is better than previous result. If not, the result is replaced within a certain probability.

Step 7. Repeat steps 4 to 6 until the end of Markov chain length at each temperature or it satisfies a certain condition.

Step 8. Repeat steps 3 to 6 until final temperature.

Step 9. Stop.

The structure of the simulated annealing algorithm is given in Fig. 1. The main difference from the precedent algorithm is that

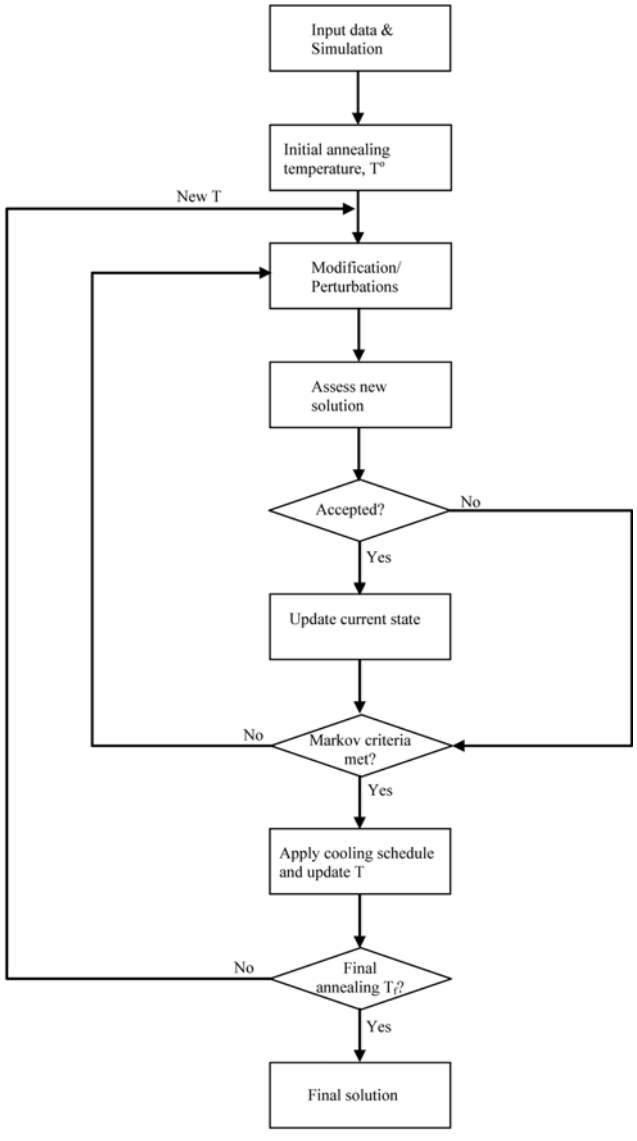

Fig. 1. The structure of the simulated annealing algorithm.

single loop of the local search algorithm is replaced by a double loop in the SA algorithm. The temperature is changed in the outer loop, and the number of neighbor moves (Markov chain length) is changed at each temperature in the inner loop. The key features of the simulated annealing algorithm are as follows, and they are briefly explained in the next section.

1. Generation of random changes
2. Markov process
3. Cooling schedule

3. Key Features of Simulated Annealing (SA)

3-1. Generation of Random Changes

Knuth developed a methodology of generating a random number to produce a new solution of the objective function [7]. This generator includes random changes and allows all possible solutions to be reached. The new solution can be produced by using the following equation, based on the random number of v, that lies between 0 and 1.

$$y' = y_{lower} + abs(y_{upper} - y_{lower}) \times \varpi \quad (1)$$

Where, y' is a new value of the perturbed variable, y_{lower}/y_{upper} are lower/upper bounds of the perturbed variable. ϖ is the random number.

A set of perturbation probabilities is applied to produce the modification of variables during optimization. For example, higher perturbation probabilities induce bigger modification of the variables. This perturbation probability enables the flexibility of the optimization. In practice, if the solution in the system is very sensitive to the optimization variables, higher probabilities must be applied to the optimization variables.

3-2. Markov Process

The simulated annealing algorithm is based on the theory of Markov chains that provides the essential background of a Monte Carlo-based algorithm.

A Markov process $\{x_n\}$ can be represented as a series of sequential events. The transition of the matrix, representing the probability of moving from i to j, is independent of its past behavior when its current state is known. The mathematical form of Markov property is formulated as follows [8].

$$T_{ij}\{x_{n+1}=j|x_n=i\} = T_{i,j}\{x_{n+1}=j|x_0=i_0 \ldots, x_{n-1}=i_{n-1}, x_n=i\} \quad (2)$$
$$\forall i_k, i\, j \in S, \forall n, k \in N_0$$

Where,

T_{ij}: transition matrix
n: a time point
i, j, i_k: states of system
S: state space

Transition probabilities from state i to j are stored in the transition matrix, T_{ij}, and the sum of the values in each row becomes unity [9].

If the transition probabilities are constant throughout the events, it is defined as a homogeneous process, while the variation of the transition probabilities with time is defined as a heterogeneous process. Simulated annealing can be described as a heterogeneous Markov process because the transition probabilities change with different annealing temperature. The transition probabilities are a function of the annealing temperature. Markov chain length is one of the important variables to be specified at the initial stage. If the chain length is unnecessarily long, it reaches a global optimum point with the extra cost of high computation time. On the other hand, too short a chain length cannot guarantee a global optimum solution. For this reason, this chain length must be carefully considered at the initial stage.

According to Dekkers and Aarts, the chain length is decided by problem dimension as follows [10]:

$$M_{CL} = 10 \times n_d \quad (3)$$

Where, n_d is dimensionality of the problem. Markov chain length increases with increased dimensionality of the problem. However, an appropriate selection of this Markov chain length is rather controversial and it should be adjusted by trying various different values [11]. In this work, various lengths were applied by trial and error in the range of 6 to 30, depending on the problem, and the most appropriate number was selected for each case.

As shown in Fig. 1, there are two loops, an inner loop and an outer loop. The inner loop is the Markov process loop and the outer loop adjusts the annealing temperature. The inner loop is terminated when the total number of modifications reaches the total Markov chain length, M_{CL}, or the number of accepted moves reaches $M_{CL}/2$. The application of the above statements allows the computation time to be reduced effectively at high temperature. In a high temperature, $M_{CL}/2$ is mostly used for the termination of the loop, because the acceptance ratio of modifications is much higher than the case of low temperature. However, longer computation time is needed to attain the global optimum solution at a low temperature.

Because the SA algorithm does not require derivative information, it merely needs to be supplied with an objective function for each trial and the solution that it generates. Thus, the evaluation of the problem functions is essentially a 'black box' operation in the perspective of the optimization algorithm. To assess the objective functions which are produced with new modified variables during optimization, acceptance criteria should be applied. The acceptance criteria proposed by Metropolis et al. are used in this work [1]. A Boltzmann distribution is used to find probability of acceptance, P_{ij} and an acceptance criterion, B_{ij} is defined as follows.

$$\Delta E_{ij} = (E_{i+1} - E_i) \quad (4)$$

$$P_{ij} = \exp(-\Delta E_{ij}/T_a) \quad (5)$$

$$B_{ij}(T_a) = \min(1, P_{ij}) \quad (6)$$

$$\forall i \neq j, i, j \in S, T_a \in R_+$$

If the change in energy is negative, all new configurations are accepted. However, if the change in energy is positive, it is accepted with a probability given by the Boltzmann factor, $\exp(-\Delta E_{ij}/T_a)$. For example, when the energy change is positive, the high temperature allows higher probabilities in the acceptance criteria. On the other hand, small value of probability in acceptance criteria is attained for low temperatures from the above equations. Once new moves are accepted, the solutions are evaluated again with regard to the constraints of the problem. By iterating all these procedures, a global solution that satisfies all design constraints can finally be attained.

3-3. Cooling Schedule

Cooling schedule is one of the most important features of the SA

algorithm. It determines the degree of uphill movement during the search. In practice, an initial temperature should be high enough to 'melt' the system completely and be decreased in some way to the 'freezing point'. However, selection of the cooling schedule for practical purposes is still something of a black art [12]. The equation of cooling schedule, introduced by Aarts and Van Laarhoven, is employed in this work as follows [13]:

$$T_a^{k+1} = T_a^k \left(1 + \frac{\ln(1+\theta)T_a^k}{3\sigma(T_a^k)}\right)^{-1} \quad (7)$$

Where,

σ: Standard deviation of the objective function
T_a^k: Annealing temperature
θ: Cooling parameter

The cooling parameter controls the rate of temperature decrease during the optimization. The temperature decrease becomes faster as the annealing parameter takes bigger values. In the meantime, the probability of being trapped in a local optimum point becomes higher with a bigger value of the annealing parameter. Typical values of the annealing parameter are between 0.01 to 1.0. In this work, a value of 0.05 is employed.

As shown in Fig. 1, the annealing temperature loop is terminated when the temperature reaches a final temperature or the modification is no longer accepted for 'm×M_{CL}'. The value of 'm' should be selected carefully, depending on the type of optimization problem. Too small a value allows that optimization is terminated while it still produces a local optimum solution. On the other hand, too high value generates unnecessarily long computation time. Mehta proposed 5 for reactor network synthesis and Choong employed 10 for batch crystallization [14,15]. In this work, a value of 3 is applied for the optimization of heterogeneous reactor designs.

PROFILE-BASED SYNTHESIS APPROACH

For industrial application of reactor and catalyst modelling and its synthesis, a number of variables should be considered simultaneously, which leads to a significant computational burden for optimization. For example, catalyst type, size, active material distribution at each stage of the reactor, operating temperature along the reactor operation period, etc. should be accounted simultaneously for the maximum performance of the reactor with high selectivity. Therefore, in some cases, it was found to be much more efficient to optimize a profile of the continuous variable which is manipulated by a set of variables rather than optimizing discrete variables within a full range boundary. For example, to produce different types of temperature profiles for a certain operation period during optimization, a mathematical equation must be applied to describe a temperature profile. This equation can be any type, such as first order, second order, exponential, asymptotic and so on. Since there are many different types of equations, it is rather inefficient and time consuming to apply every single possible equation in the model. Therefore, a profile-based synthesis approach has been applied to the work. Metha and Kokossis applied it to generate optimized temperature profiles through the axis of a reactor [16]. However, there were some limitations to describe specific types of profiles. Therefore, Choong later extended this method to cover a broader range of profiles [15].

In principle, Eqs. (8) and (9) allow various types of profiles to be generated by combining two different types of profiles, exponential and asymptotic curves. The first profile in Eq. (8) is an exponential curve and the second profile in Eq. (9) is an asymptotic curve.

Type I (exponential curve)

$$Z(s) = Z_1 - (Z_1 - Z_2)\left(\frac{S}{S_{total}}\right)^{A_2} \quad (8)$$

Type II (asymptotic curve)

$$Z(s) = Z_2 - (Z_2 - Z_1)\left(\frac{S_{total} - S}{S_{total}}\right)^{A_1} \quad (9)$$

Where,

S: pellet location within pellet length
Z: Volumetric activity value
Z_1: Inlet value
Z_2: Outlet value

To generate every feasible shape of profile, the two curves are tied together at a certain point and height inside a pellet, for example. This tied-in point is controlled by two variables (TB_1 and Z_3). Also, the slope of each curve is controlled by variables A_1 and A_2. In this case, four to six variables are manipulated to generate various profiles with fixed initial and final points. The type of profile is determined by the variables A_1, A_2, TB_1, Z_1, Z_2 and Z_3.

A_1: The power of equation type II ($A_1 \geq 1$)
A_2: The power of equation type I ($A_2 \geq 1$)
Z_3: The volumetric activity value corresponding to TB_1 (value between 0 and 1/3 for sphere, 1/2 for cylinder and 1 for slab)
TB_1: Intermediate peak point for the curve ($-1 < TB_1 < 0$ for Type I+ Type II, $0 < TB_1 < 1$ for Type II+Type I)

The application is applied to case studies which will be described in Section 5.

MODELLING OF HETEROGENEOUS CATALYTIC REACTOR

1. Heterogeneous Catalytic Reactor

Heterogeneous catalytic reactors have been workhorses in the large-scale chemical product industry. Fixed-bed reactors have been preferred because of relatively low cost and simplicity of application compared with fluidized-bed or moving bed reactors. Fixed-bed reactors have been increasingly used in recent years, especially in gas-phase reactions. They can be categorized into several different configurations according to applications, as follows [17].

• Single adiabatic reactor: exothermic or endothermic non-equilibrium limited reaction (e.g., mild hydrogenation process).

• Adiabatic bed reactors in series with intermediate heat exchange: high conversion, equilibrium-limited reactions (e.g., SO_2 oxidation, catalytic reforming, ammonia synthesis and hydro-cracking processes).

• Multi-tubular non-adiabatic reactors: highly endothermic or exothermic reactions requiring close temperature control to obtain high selectivity (e.g., hydrogenation and oxidation process).

• Direct-fired non-adiabatic reactors: highly endothermic reactions with high temperatures (e.g. steam reforming process).

Mass and energy balances used for the design of the heterogeneous catalytic reactor are described below.

For the Bulk/Fluid Phase:

The fluid phase mass and energy balances for heterogeneous, non-isothermal, non-adiabatic plug flow reactors are shown below.

- Mass balance

$$\nu\frac{dC_{f,i}}{dz} = -(1-\varepsilon)\cdot\sum(\upsilon_{i,j}\cdot r_j) \tag{10}$$

- Energy balance

$$\rho c_p \nu\frac{dT_f}{dz} = (1-\varepsilon)\sum(-\Delta H_j\cdot r_j) - U_o\alpha(T_f - T_c) \tag{11}$$

- Boundary condition,

$$z=0:\ T_f = T_f^o,\ C_{f,i} = C_{f,i}^o \tag{12}$$

Where, ν=velocity of external fluid phase
$C_{f,i}$=fluid concentration on species in bulk phase, I
Z=axial co-ordinate along the reactor
ε=bed void fraction
$\nu_{i,j}$=stoichiometric coefficient of species, i in reaction j
r_j=rate of reaction, j
ρ=density of fluid phase
C_p=heat capacity of fluid phase
ν=velocity of external fluid phase
T_f=temperature of fluid phase
ΔH_j=heat of reaction j
U_o=overall heat transfer coefficient between reaction gases and cooling medium
α=4/D_t (internal tube diameter)

For the Fluid/Particle Interface:

The mass and energy balances in catalyst phase with external transfer resistances are shown below.

- Mass balance

$$k_{g,i}(C_{s,i} - C_{f,i}) = -D_{e,i}\frac{dC_i}{dx} = \eta\sum(\upsilon_{i,j}\cdot r_{s,j})\rho_p S' \tag{13}$$

- Energy balance

$$h(T_s - T_f) = -\lambda\frac{dT}{dx} = \eta\sum(\Delta H_j\cdot r_{s,j})\rho_p S' \tag{14}$$

Where, $k_{g,i}$=external mass transfer coefficient of component I
$C_{s,i}$=fluid concentration on species on the surface of the catalyst, I
$D_{e,i}$=effective diffusivity coefficient of component, I
x=distance from pellet centre to surface
η=effectiveness factor
$r_{s,j}$=rate of reaction, j on catalyst surface
ρ_p=density of pellet
S′=characteristic pellet length (=Vp/Sp)
V_p=volume of pellet
S_p=surface of pellet
h=external heat transfer coefficient
T_s=temperature of catalyst surface
T_f=temperature of fluid phase
λ=effective thermal conductivity

For the Catalyst Particle:

The mass and energy balances in catalyst phase with internal diffusional resistances are shown below.

- Mass balance

$$D_{e,i}\left[\frac{1}{x^n}\frac{d}{dx}\left(x^n\frac{dC_i}{dx}\right)\right] = \sum(\upsilon_{i,j}\cdot r_j)\cdot a(x) \tag{15}$$

- Energy balance

$$\lambda\left[\frac{1}{x^n}\frac{d}{dx}\left(x^n\frac{dT}{dx}\right)\right] = -\sum[(-\Delta H_j)\cdot r_j]\cdot a(x) \tag{16}$$

- Boundary condition

$$x=0;\ \frac{dC_i}{dx} = \frac{dT}{dx} = 0$$

Where,
x=1; $C_i = C_{s,i}$, $T = T_s$
n=integer characteristic of pellet geometry
n=0 for infinite slab; n=1 for infinite cylinder; n=2 for sphere
a(x)=1 for uniform catalyst
C_i=concentration of component I
a(x)=activity distribution function

In this work, a plug-flow packed-bed reactor is regarded as a number of sub-PFRs in series. To increase computational efficiency of the optimization problem, effectiveness factor is obtained at the inlet of each sub-PFR and applied to the sub-PFR's. In the meantime, the accuracy of the heterogeneous catalytic reactor model and computational requirements for optimization are controlled by manipulating the number of sub-PFRs. This method allows producing more

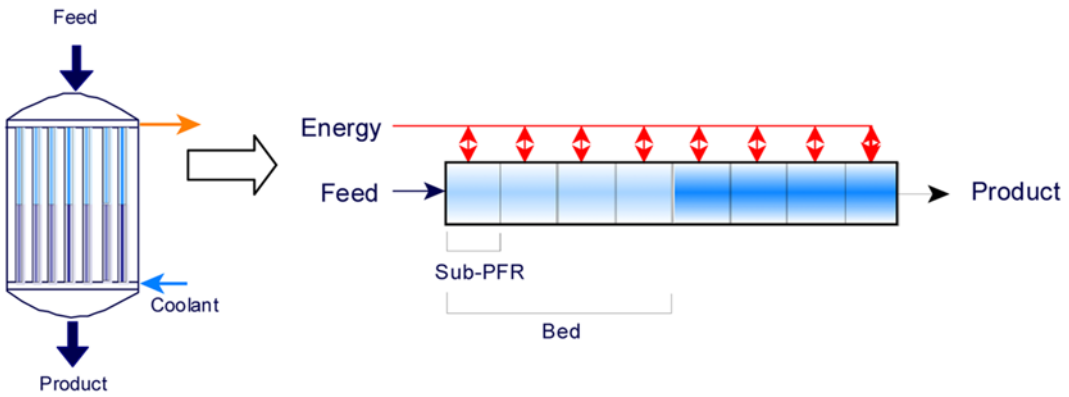

Fig. 2. Schematic non-isothermal and non-adiabatic reactor design with different catalyst dilution in two bed zones.

accurate results of the model within a reasonable optimization time. The equations above are applied to the mass and energy balances of the fluid phase, internal and external catalyst phases [18-20]. A reactor is divided into several bed zones which are arranged with different types of catalysts, and a set of sub-PFRs represents a bed zone inside a reactor. By using this method, various reactor designs can be considered. For example, any number of reactor beds can be specified and different degrees of catalyst dilution can be applied to each bed, as described in Fig. 2. For the modelling of a multi-tubular reactor, the number of tubes, the length and diameter of each tube must be specified in order to calculate heat exchange area, which plays a critical role in non-isothermal reactions. Furthermore, inlet coolant temperature, reactor volume, injection type of coolant, heat transfer coefficient, etc. should be applied in reactor modelling.

Pellet Size and Shape:

Pellet size must be considered at the reactor design stage. As shown in Eqs. (17) and (18), the pellet size is closely related to the Thiele modulus and the effectiveness factor. For example, this correlation can be deduced from Eq. (15) in a dimensionless form [18].

$$\frac{d^2y'}{ds^2} = -\frac{n}{s}\frac{dy'}{ds} + \varphi^2\rho_p\sum(-\upsilon_{i,j}\cdot f_j) \tag{17}$$

Where, φ^2 is the Thiele modulus:

$$\varphi^2 = \frac{R_{s,i}R_p^2}{D_{e,i}C_{s,i}} \tag{18}$$

Where, y' is concentration fraction, ρ_p is density of pellet, ν_{ij} is stoichiometric coefficient of species, i in reaction j and $D_{e,i}$ is effective diffusivity of component i.

The pellet size is also optimized along the reactor axis to control the activities of the different catalyst beds. In general, a high activity can be obtained from a small pellet, while activity drops as the catalyst dimension increases due to high diffusional resistances inside a pellet. However, if the pellet becomes too small, the pressure drop may increase beyond the allowable pressure drop of the reactor. Therefore, the pressure drop must be carefully monitored as the pellet dimensions vary.

To consider various shapes of pellets for the calculation of the effectiveness factor, characteristic pellet shape and dimension parameters were developed by Aris [21]. This characteristic pellet dimension number is calculated as a ratio of pellet volume to surface area, and pellet shape number ranges between 0 (infinite slab) and 2 (sphere). However, this allows only one pellet dimension to characterize the pellet shape, while the pellet length of the catalyst is assumed to be infinite. For this reason, the method applies only to spherical type of catalyst, providing results with reasonable accuracy since this is the only shape that has one pellet dimension. To compensate for the weakness, Burghardt and Kubaczka developed a new method [22]. For example, a new characteristic pellet shape and dimension numbers were developed based on three dimensions of the pellet in order to consider the impact of geometrical pellet shape on its activity. These new characteristic pellet shape and dimension numbers are employed to this work to obtain more accurate catalyst effectiveness factors. The detailed calculation procedure can be found in the paper of Burghardt and Kubaczka [22].

Effectiveness Factor:

The catalyst performance can be defined by an effectiveness factor and described by the following equation [23].

$$\eta_j = \frac{\int_0^1 f_j a(s)s^n ds}{\int_0^1 a(s)s^n ds} \tag{19}$$

Where, η is effectiveness factor, f_j is dimensionless reaction rate j, a is activity distribution function and s is dimensionless catalyst phase co-ordinate.

Eqs. (10)-(16), with $C_{f,i}$, T_f solved from the differential equations along the reactor axis, the unknown variables $C_{s,i}$, T_s in each section of the plug-flow reactor and the C_i, T profile within the pellet, were solved continuously using a non-linear equation solver. Eqs. (15) and (16) were solved as a two point boundary-value problem using a Runge-Kutta-Merson method and a solver in a shooting and matching technique (NAG Fortran Library, D02HAF).

The heterogeneous reactor model offers higher accuracy for the design of the reactor. On the other hand, it suffers from the lack of catalyst related data including heat transfer and diffusional resistances. It is also computationally more demanding than a pseudo-homogeneous model. Therefore, the pseudo-homogeneous model is more applicable for conceptual reactor design in the early stage, whereas a heterogeneous model is followed for rigorous analysis.

Mixing Rule of Inert Catalyst:

The inert fraction at reactor bed is defined as follows:

$$\alpha' = \frac{V_{diluted}}{V_{diluted} + V_{undiluted}} \tag{20}$$

Inert fraction is multiplied to the bulk density of pure catalyst mixture in each bed and used for the mass and energy balance equations through the reactor axis [24-26].

For the modelling of the catalyst bed, an assumption of even fluid distribution across the bed is used [27]. For example, perfect homogeneous mixing of both the inert particles and the catalyst particles is not possible due to their finite dimensions and changes in residence time distribution occur. These effects decrease with increasing ratio of bed length to particle diameter. However, this behavior is not considered in this work.

Superstructure of Reactor Model:

For the design of feed stream distribution, mass and heat balance of the side and main streams inside a reactor should be considered. As described in Fig. 3, the reactor model comprises a number of sub-PFRs. Each sub-PFR should be allowed to be connected with a side-stream in a superstructure, satisfying the mass and energy balance during optimization. The superstructure of all stream connections between side and main streams is built by using a flag function. The general procedure for simulation and optimization of reactor design is illustrated in Fig. 3.

This method enhances conceptual reactor design by considering a number of various configurations of side or main streams and catalyst dilution during optimization. A penalty function is used to optimization algorithm in order to keep the temperature profile of reactor within allowable range along the reactor axis during optimization.

1-1. Non-uniform Catalyst

Many researchers have demonstrated that various types of non-uniform activity distribution profiles can be generated by using impregnation techniques. Maatman illustrated the use of co-impregnation as a means of controlling the active catalyst material distri-

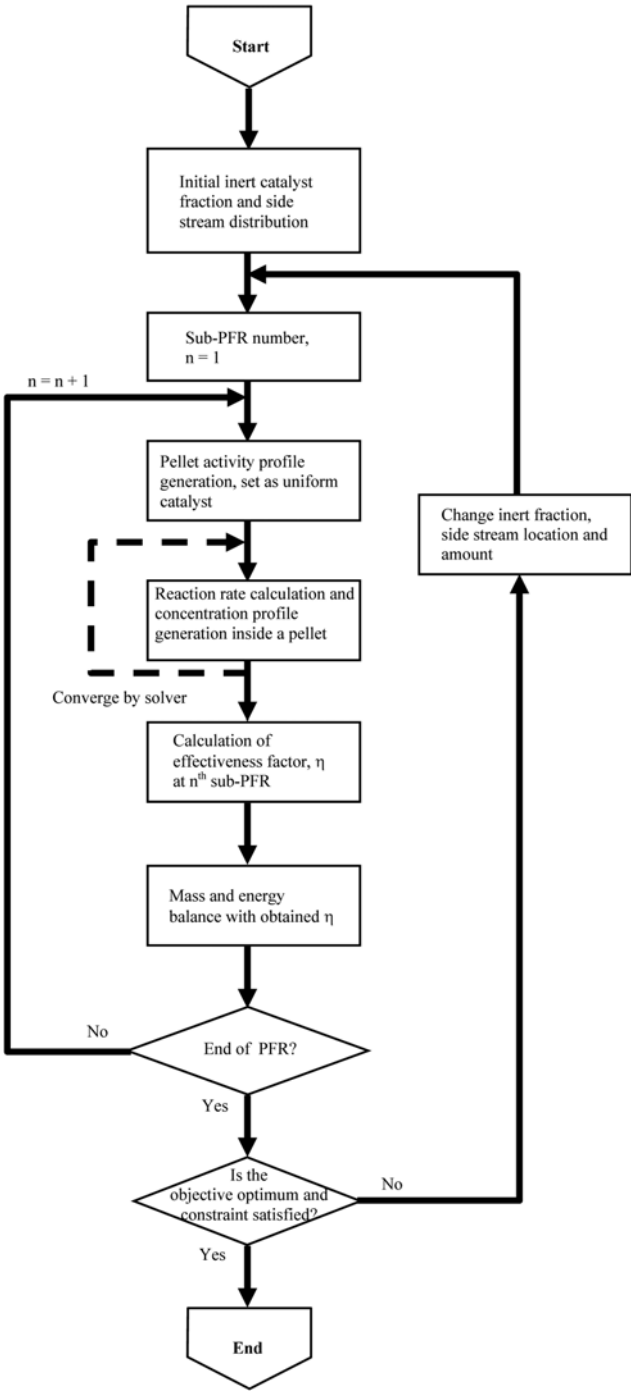

Fig. 3. The algorithm for reactor design simulation and optimization.

bution in a pellet for the case of platinum deposition from chloroplatinic acid on alumina support [28]. Since then, co-impregnation techniques have been widely used to prepare non-uniformly distributed catalysts. Shyr and Ernst showed that numerous types of non-uniform catalyst pellet profiles could be prepared by using impregnation techniques [29]. In their works, different types of chemical additives (co-ingredients), chemical additive concentration and impregnation time were controlled to produce various non-uniform Pt activity distribution profiles in spherical γ-alumina beads. Their research

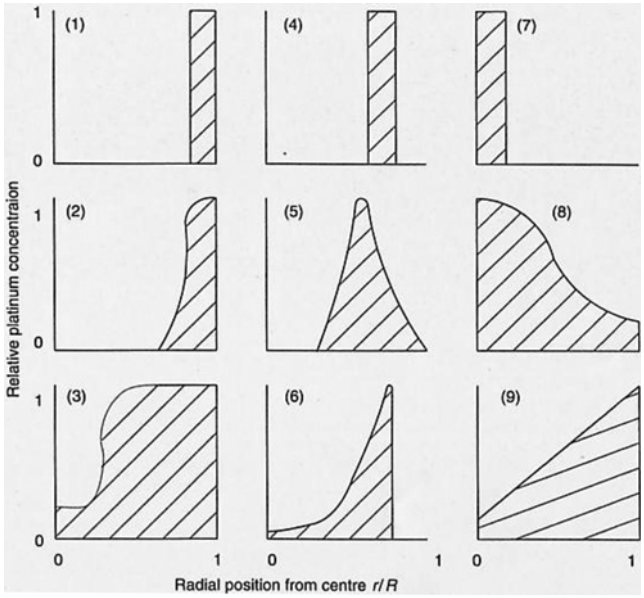

Fig. 4. Types of Pt profiles obtained by co-impregnation (reproduced from Journal of Catalysis, 1980, 63, 425).

used HCl, HF, HNO_3, acetic acid, citric acid, tartaric, $AlCl_3$, NaCl, NaF, NaBr, $NaNO_3$, Na_3PO_4, Na benzoate, and Na citrate. Two different impregnation times were used (1 hour and 22 hours). The results showed nine different types of pellets as a result, as described in Fig. 4.

These experiments demonstrate that various types of active material distribution profile can be manufactured once a specific type of optimal profile has been designed. Furthermore, the location of active material distribution inside a pellet changes according to the impregnation time.

1-2. Modelling Of Non-uniform Catalyst

To describe the non-uniform distribution inside a catalyst pellet, the activity distribution factor is introduced. The a(x) in Eqs. (15) and (16) must satisfy the normalization condition [30].

$$\frac{1}{V_p}\int_{V_p} a(x)\,dV_p = 1 \tag{21}$$

The above equations can be converted into a dimensionless form by introducing the variables:

$$s = \frac{x}{R_p},\ f_j = \frac{r_j}{r_{s,j}}$$

Where, V_p is volume of pellet p, a is activity distribution function, s is dimensionless catalyst phase co-ordinate, x is distance from pellet center to surface, R_p is radius of pellet and r is rate of reaction, j.

Furthermore, Eq. (21) can be expressed in a general form:

$$\int_0^1 a(s)s^n ds = \frac{1}{n+1} \tag{22}$$

Where, n is integer characteristic of pellet geometry, number of sub-PFR (n=0 for infinite slab; n=1 for infinite cylinder; n=2 for sphere).

By combining the above equations with Eq. (19), the effective-

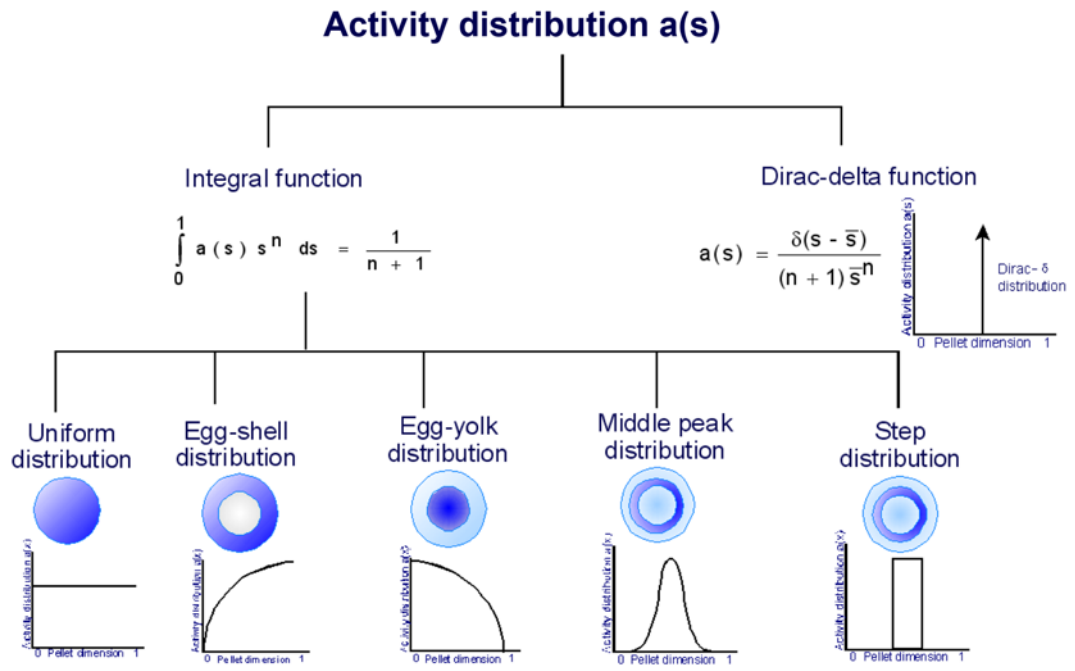

Fig. 5. Activity distribution profile examples for non-uniform catalyst.

ness factor of non-uniform activity distribution profile inside a pellet is produced, and it is applied to energy and mass balance equations at each sub-PFR.

The integration of activity profiles through the pellet volume at certain type of pellet, such as slab, cylinder and sphere can be carried out by using Eq. (22). Since inlet and outlet values of each shape of catalyst are fixed, only the shape of the integrated activity profile can be changed during optimization between two fixed values. After a certain type of profile has been generated, the corresponding profile is transformed to an activity distribution profile through the pellet. Lastly, the concentration profiles of all components inside a pellet are generated based on the second-order boundary value problem, and they are used to generate an appropriate effectiveness factor. Typical volumetric activity profiles of spherical catalyst involving egg-yolk, egg-shell and middle peak type are shown in Fig. 6.

For an optimization of activity distribution profile, various volu-

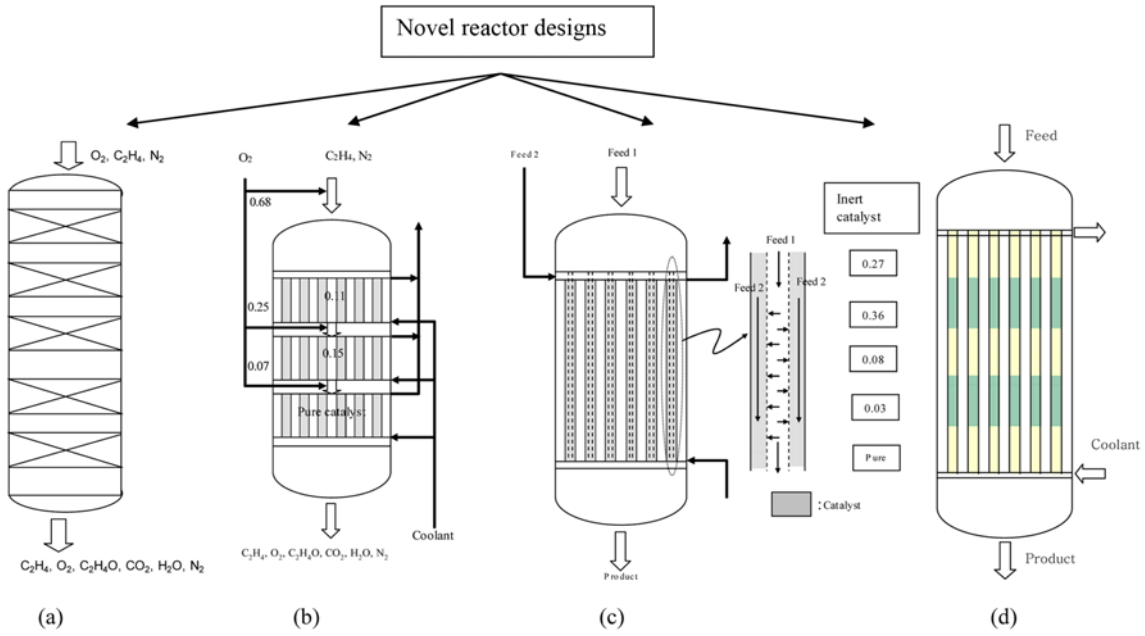

Fig. 6. Example of reactor design configurations: (a) Five-bed reactor with optimum inert catalyst mixing, (b) Three-bed and multi-tubular reactor with optimum inert catalyst mixing and ethylene side stream, (c) Packed-bed membrane reactor, (d) Five-bed multi-tubular reactor configuration with inert and surface layered catalyst mixing.

metric activity profiles for a spherical type of pellet and the corresponding activity distribution profile inside a pellet are generated through a profile-based synthesis approach.

Typical non-uniform catalysts are briefly summarized in Fig. 5. Further detailed discussion about mathematical modelling of each type of non-uniform catalyst is illustrated by Hwang [31].

APPLICATION

1. Ethylene Oxidation Process

Ethylene oxide is produced by vapor-phase oxidation of ethylene with oxygen or air on a supported silver catalyst. In general, the composition of the feed stream contains 5 to 10 vol% ethylene and 5 to 10 vol% oxygen as reactants, and nitrogen is typically used as an inert gas. Organic coolant is generally used as a cooling medium. The optimum temperature inside a reactor is generally around 230 °C and the selectivity ranges between 70 to 80 percent when pure oxygen is used instead of air [32].

The reaction kinetics is obtained from the work of Klugherz and Harriott [33]. These have previously been employed for the study of Dirac-delta catalysts by Morbidelli et al. and Baratti et al. [18, 34]. The effective diffusivity coefficients are obtained from Satterfield, and thermal conductivity of alumina pellets are obtained from Mischke and Smith [32,35]. External heat and mass transfer coefficients are obtained from the data of Baratti et al. [18].

Reaction 1

$$C_2H_4+\frac{1}{2}O_2\rightarrow C_2H_4O \qquad \Delta H=-120{,}036\ \text{kJ/kmol} \qquad (23)$$

Reaction 2

$$C_2H_4+3O_2\rightarrow 2CO_2+2H_2O \qquad \Delta H=-1{,}324{,}280\ \text{kJ/kmol} \qquad (24)$$

$$r_1=k_1c_1c_2^2/F_1^2$$
$$r_2=k_2c_1c_2^2/F_2^2$$
$$F_1=(0.0106+2144c_1+805c_2)\cdot(1+1271\sqrt{c_2})$$
$$F_2=(0.008+4166c_1+1578c_2)\cdot(1+718\sqrt{c_2})$$
$$k_1=k_1^0\exp[\gamma_1(\theta-1)/\theta]$$
$$k_2=k_2^0\exp[\gamma_2(\theta-1)/\theta]$$

The above reaction is a typical industrial ethylene oxidation process, and the related computational data are given in Table 1.

Reactor design data is taken from the reports of ethylene oxide revamping projects by Coombs et al. and Huang et al. [36,37]. The data are as follows:

Reactor size
- Tube diameter=0.03912 m
- Tube length=12.8 m
- Tube material=Carbon steel
- Number of tubes=2781

Table 1. Computational parameters for the ethylene oxide process

$k_1^o=8.63\times10^6$ mol/s cm^3	$R_p=0.25$ cm, n=2
$k_2^o=6.57\times10^6$ mol/s cm^3	Silver catalyst
$D_{e,1}=0.003$ cm^2/s	$x_{f,1}^o=0.08$, $x_{f,2}^o=0.06$, $x_{f,3}^o=0.86$
$D_{e,2}=0.004$ cm^2/s	$k_{g,1}=4.5$ cm/s, $k_{g,2}=5.44$ cm/s
$\gamma_1=21.9$, $\gamma_2=29.7$	$\lambda=2.2e^{-4}$ kW/m·K, h=0.88 kW/m^2·K

- Total heat transfer area=4396 m^2
- Overall heat transfer coefficient=0.176 kW/m^2 K
- Total reactor volume=43 m^3
- Catalyst density=881 kg/m^3
- Catalyst per reactor=9,431 kg

Feed molar flow (kmol/hr)
- Ethylene=100
- Nitrogen=1075
- Carbon dioxide/ Ethylene oxide/ Water=0
- Oxygen=75

In general, bigger size of pellet and inner location of active material

Table 2. Summary of various reactor designs in ethylene oxidation

	Case 1	Case 2	Case 3	Case 4
Yield (%)	39.2	45.7	45.4	32.4
Yield increase (%)	-	16.6	15.8	−17.3
Selectivity (%)	74.7	71.7	71.0	74.0
Ethylene oxide product (kmol/hr)	31.5	36.8	36.5	35.9
Maximum temperature (°C)	224	231	234	225
	Case 5	Case 6	Case7	Case 8
Yield (%)	42.0	45.5	44.6	45.5
Yield increase (%)	7.2	16.1	13.8	16.1
Selectivity (%)	74.1	73.2	72.7	72.2
Ethylene oxide product (kmol/hr)	33.8	36.6	35.9	36.6
Maximum temperature (°C)	226	229	228	230
	Case 9	Case 10	Case 11	
Yield (%)	45.0	48.0	46.6	
Yield increase (%)	14.8	22.4	18.9	
Selectivity (%)	72.8	71.7	71.4	
Ethylene oxide product (kmol/hr)	36.2	38.6	37.5	
Maximum temperature (°C)	228	231	237	

Case 1: Base case
Case 2: Five-bed tubular reactor with optimum inert catalyst mixing
Case 3: Three-bed and multi-tubular reactor with optimum inert catalyst mixing and ethylene side stream
Case 4: Packed-bed membrane reactor
Case 5: One-bed reactor with surface layered catalyst (10% thickness)
Case 6: Three-bed reactor with optimum active material location inside Dirac-d catalyst
Case 7: Three-bed reactor with optimum active material location inside layered catalyst (10% thickness)
Case 8: Three-bed reactor with optimum active material location obtained from profile based synthesis (PBS)
Case 9: Three-bed reactor with optimum pellet size with surface layered catalyst (10% thickness)
Case 10: Five-bed tubular reactor under optimum inert catalyst mixing with pure surface layered catalyst (10% thickness)
Case 11: Three-bed and multi-tubular reactor under optimum inert catalyst mixing with pure surface layered catalyst (10% thickness) and oxygen sidestream

generate low activity. However, this characteristic can be beneficially applied for the control of temperature inside a reactor. The heat gradient inside a pellet adds complexity to predict the activity at certain conditions, since the reaction rate is very sensitive to local temperature inside a pellet. Furthermore, in a particular case of the ethylene oxidation reaction, it was found that the use of small size of catalyst pellet or active material distribution near the catalyst surface produced higher selectivity at the same operating conditions. Under these complex conditions, various reactor and catalyst parameters below were optimized in a multi-bed tubular reactor.

1. Non-uniform catalyst
   a. Surface layered catalyst
   b. Dirac-delta catalyst
   c. General non-uniform catalyst (egg-yolk, egg-shell, middle-peak, etc.)
   d. Layered catalyst
2. Number of reactor beds
3. Pellet dimension
4. Reactor configuration (side stream distribution, inert catalyst mixing, membrane reactor)

For the optimization of reactor and catalyst synthesis, simulated annealing is initially applied to produce a set of reasonable solutions and each solution is further optimized by using a deterministic algorithm.

Table 2 shows the summary of the optimization results based on different combinations of the above variables for the synthesis of heterogeneous catalytic reactor, and some examples of feasible reactor designs are shown in Fig. 6.

In this work, 70% of minimum selectivity was used as a constraint for the maximization of yield. In total, 11 different types of reactor configurations are produced after optimization. For example, the maximum yield of 48%, which shows 22.4% increase, is achieved by using a combination of inert catalyst mixed with surface layered catalyst in a five-bed tubular reactor.

Furthermore, it was observed during the analysis of optimization results that selectivity decrease could be minimized by using a thin layered active material distribution on the catalyst surface rather than uniform active material distribution particularly in ethylene oxidation process.

CONCLUSION

Optimum synthesis of a heterogeneous catalytic reactor has been achieved through the combination of simulated annealing and deterministic optimization. It was observed that the application of simulated annealing is more effective for the design of reactor and catalyst, and its synthesis because of its capability to provide a set of good solutions which meet an objective function in a fixed amount of time rather than one best possible solution. Therefore, this method can be used as a targeting tool as well as an analysis tool so that a design engineer can evaluate several feasible system designs as an alternative option. Furthermore, the stochastic algorithm has been proven to be much more powerful in avoiding any trap from local optima.

Clearly, long computational time has been a significant drawback for a simulated annealing process. Therefore, a deterministic optimization is applied at the late stage of optimization to avoid unnecessary delay in reaching a final optimum solution. Furthermore, profile-based synthesis is adopted to reduce complexity burden. In this study, manipulation of only a few set of variables allowed generation of various types of different profiles, and it was proved that this methodology greatly enhanced the efficiency of optimization.

Synthesis of heterogeneous catalytic reactors has been reviewed with industrial application by covering the following items.

- Novel configuration of reactor system (side stream distribution, inert catalyst mixing, membrane reactor, etc.)
- Modelling of catalyst with infinite dimension and its shape.
- Non-uniform catalyst (Dirac-delta, profile synthesis, layer type)
- Catalyst deactivation

For industrial application, the ethylene oxidation process is illustrated with the optimization results, showing a variety of feasible design alternatives to a design engineer. Furthermore, the optimization results proved significant increase of yield and selectivity in ethylene oxidation process.

NOMENCLATURE

A_1 : the power of equation type II
A_2 : the power of equation type I
$a(x)$: activity distribution function
$a_{d,j}$: catalyst deactivation function
B_{ij} : acceptance probability from the state (i) to (j)
C_i : concentration of component i
C_p : heat capacity of fluid phase
$C_{f,i}$: fluid concentration on species in bulk phase, i
$C_{s,i}$: fluid concentration on species on the surface of the catalyst, i
$D_{e,i}$: effective diffusivity coefficient of component, i
$E_{i,f}$: objective function
h : external heat transfer coefficient
$k_{g,i}$: external mass transfer coefficient of component i
M_{CL} : Markov chain length
n_d : dimensionality of the problem
P_{ij} : acceptance probability from state (i) to (j)
r_j : rate of reaction, j
$r_{s,j}$: rate of reaction, j on catalyst surface
R_p : radius of pellet
S : state space
s : dimensionless catalyst phase co-ordinate
S' : characteristic pellet length (=Vp/Sp)
T, T_a : annealing temperature, local temperature inside a pellet
t : reactor operation time or catalyst cycle period
T_a^o : initial annealing temperature
TB_1 : intermediate peak point for the curve
T_c : temperature of surrounding coolant
T_f : final annealing temperature, temperature of fluid phase
T_s : temperature of catalyst surface
T_{ij} : transition matrix
U_o : overall heat transfer coefficient between reaction gases and cooling medium
V : volume
V_p : volume of pellet
x : control variable, distance from pellet centre to surface
y' : new value of the perturbed variable
y_{lower} : lower bound of the perturbed variable

y_{upper} : lower bound of the perturbed variable
Z : axial co-ordinate along the reactor, volumetric activity value
Z_1 : inlet volumetric activity value
Z_2 : outlet volumetric activity value
Z_3 : the volumetric activity value corresponding to TB1

Subscripts

i, j, k : states of system
n : time point, integer characteristic of pellet geometry (n=0 for infinite slab; n=1 for infinite cylinder; n=2 for sphere)

Superscripts

c : coolant
f : fluid phase
i : component
j : reaction
p : pellet
o : initial condition
s : catalyst surface

Greek Letters

α : $4/D_t$
α' : inert volume fraction
ΔH : heat of reaction
δ : deviation of two objective functions located at different states
ε : bed void fraction
η : effectiveness factor
φ : Thiele Modulus ($=R_p\sqrt{\frac{r_{s,j}}{D_{e,i}C_i}}$)
λ : effective thermal conductivity
ν : velocity of external fluid phase
$\nu_{i,j}$: stoichiometric coefficient of species, i in reaction j
θ : cooling control parameter
ρ : density of fluid phase
ρ_p : density of pellet
σ : standard deviation of the objective function
ϖ : random number

REFERENCES

1. N. Metropolis, A. W. Rosenbluth, M. N. Rosenbluth, A. H. Teller and E. Teller, *J. Chem. Phys.*, **21**(6), 1087 (1953).
2. M. Pincus, *Oper. Res.*, **18**, 1225 (1970).
3. S. Kirkpatrick, C. D. Gelatt and Jr. M. P. Vecchi, *Science*, **220**, 671 (1983).
4. R. W. Eglese, *European J. Operational Research*, **46**, 271 (1990).
5. F. Glover and H. J. Greenberg, *European J. Operational Research*, **39**, 119 (1989).
6. P. J. M. Van Laarhoven and E. H. L. Aarts, Simulated Annealing: Theory and Applications, Reidel, Dordrecht (1987).
7. D. E. Knuth, *The art of computer programming*, Vol. II (2nd Ed.), Addison-Wesley, London (1981).
8. H. M. Taylor and S. Karlin, *An introduction to stochastic modelling* (3rd Ed.), Academic Press, London (1998).
9. M. Iosifescu, Wiley Series in Probability and Mathematical Statistics: Finite Markov process and their applications, John Wiley and Sons Ltd. (1980).
10. A. Dekkers and E. Aarts, *Mathematical Programming*, **50**(3), 367 (1991).
11. E. C. Marcoulaki, Ph.D. Thesis, UMIST, UK (1998).
12. D. G. Bounds, *Nature*, **329**, 215 (1987).
13. E. H. L. Aarts and P. G M. Van Laarhoven, *Philips J. Res.*, **40**(4), 193 (1985).
14. V. L. Mehta, Ph.D. Thesis, UMIST, UK (1998).
15. K. L. Choong, Ph.D. Thesis, UMIST, UK (2002).
16. V. L. Metha and A. Kokossis, *Com. Chem. Eng.*, **21**(S1), S325 (1997).
17. H. F. Rase, *Fixed-bed reactor design and diagnostics*, Butterworths (1990).
18. R. Baratti, A. Gavriilidis, M. Morbidelli and A. Varma, *Chem. Eng. Sci.*, **49**(12), 1925 (1994).
19. M. M. J. Quina and R. M. Ferreira, *Ind. Eng. Chem. Res.*, **38**, 4615 (1999).
20. M. M. J. Quina and R. M. Ferreira, *Chem. Eng. Sci.*, **55**, 3885 (2000).
21. R. Aris, *Chem. Eng. Sci.*, **6**(6), 262 (1957).
22. A. Burghardt and A. Kubaczka, *Chem. Eng. Proc.*, **35**, 65 (1996).
23. M. Morbidelli, A. Gavriilidis and A. Varma, Reactors, and membranes, Cambridge University Press (2001).
24. M. M. J. Quina and R. M. Ferreira, *Ind. Eng. Chem. Res.*, **38**, 4615 (1999).
25. M. M. J. Quina and R. M. Ferreira, *Chem. Eng. J.*, **75**, 149 (1999).
26. M. M. J. Quina and R. M. Ferreira, *Chem. Eng. Sci.*, **55**, 3885 (2000).
27. C. M. Van Den Bleek, K. Van Der Wiele and P. J. Van Den Berg, *Chem. Eng. Sci.*, **24**, 681 (1969).
28. R. W. Maatman, *Ind. Eng. Chem.*, **51**(8), 913 (1959).
29. Y. Shyr and W. R. Ernst, *J. Catal.*, **63**, 425 (1980).
30. Y. C. Yortsos and T. T. Tsotsis, *Chem. Eng. Sci.*, **37**(9), 1436 (1982).
31. S. Hwang, Ph.D. Thesis, UMIST, UK (2003).
32. C. N. Satterfield, Chemical Engineering Series, *Heterogeneous Catalysis in Practice*, McGraw-Hill (1980).
33. P. D. Klugherz and P. Harriott, *AIChE J.*, **17**, 856 (1971).
34. M. Morbidelli, A. Servida, R. Paludetto and S. Carra, *J. Catal.*, **87**, 116 (1984).
35. R. A. Mischke and J. M. Smith, *Ind. Eng. Chem. Fundam.*, **1**, 288 (1962).
36. J. Coombs, D. Kim and L. Palombo, *Report of ethylene oxide reactor revamp*, Department of Chemical Engineering, Rice University (1997). http://www.owlnet.rice.edu/~ceng403/ethox97.html
37. J. Huang, D. Resendez and G. Tran, *Ethylene Oxide Reactor System*, Department of Chemical Engineering, Rice University, (1999). http://www.owlnet.rice.edu/~ceng403/gr1599/finalreport3.html